RSC Advances

ROYAL SOCIETY OF CHEMISTRY

www.rsc.org/advances

ZnFe2O4 nanoparticles and clay encapsulated ZnFe2O4 nanocomposite; synthesis strategy, structural characteristics and adsorption of dye pollutants in water

Azadeh Tadjarodi*, Mina Imani, Mohammad Salehi

Research Laboratory of Inorganic Materials Synthesis, Department of Chemistry, Iran University of Science and Technology, Narmak, Tehran, 16846-13114, Iran

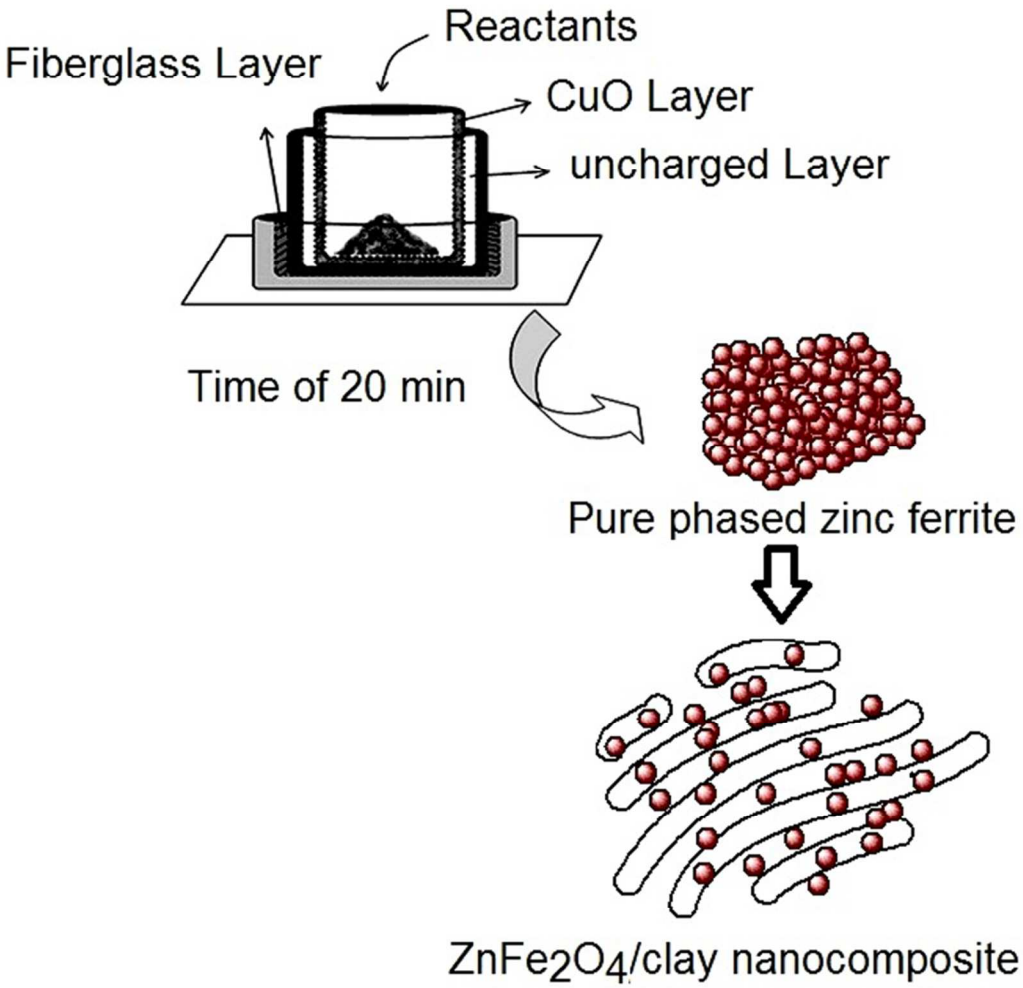

$ZnFe_2O_4$ nanoparticles and clay encapsulated $ZnFe_2O_4$ nanocomposite; synthesis strategy, structural characteristics and adsorption of dye pollutants in water

Azadeh Tadjarodi[1*], Mina Imani, Mohammad Salehi

Research Laboratory of Inorganic Materials Synthesis, Department of Chemistry, Iran University of Science and Technology, Narmak, Tehran, 16846-13114, Iran

[1*]Corresponding Author:

Email: tajarodi@iust.ac.ir (A. Tadjarodi)

Tel: +98(21) 77240516

Fax: +98(21) 77491204

Abstract

In this work, zinc ferrite nanoparticles were prepared by a one-pot microwave assisted combustion in solid state with a controllable power up to 900 W and tunable time up to 20 min. Then, $ZnFe_2O_4$ nanoparticles were encapsulated in organoclay by ultrasound assisted impregnation to obtain zinc ferrite/organoclay nanocomposite as magnetic heterostructured adsorbent. The combustion reactions were operated in a reaction set-up manufactured from an alumina crucible encircled by a jacket of CuO as microwave absorbing layer. This work-piece absorbs the distributed microwaves and supplies calcination conditions without any external heat source to prepare a pure phase of zinc ferrite. The effect of microwave power and time parameters on structural and morphological features of the samples were discussed in detail. The adsorption performance of the products for water purification of some dye pollutants was also studied. The UV-Vis results showed that the addition of as-prepared magnetic nanoparticles on the exfoliated organoclay considerably increased the adsorption of organic dye pollutants from aqueous solution. Magnetic hysteresis measurements were performed on a vibrant sample magnetometer (VSM) showing the soft paramagnetic property of the resulting products at room temperature. The structural and morphological analyses were also investigated in detail.

Keywords: Zinc ferrite; Organoclay; Nanocomposite; Microwave; Adsorption.

1. Introduction

The discharge of toxic dye wastewaters to environment from industrial activities is a major environmental problem for water bodies. They are carcinogenic and toxic to ecosystem and strongly

threaten the survival of organisms. Therefore, elimination of these hazardous pollutions from water bodies and refinement of wastewater by a reasonable route is vital.[1-3] Adsorption has been found to be an efficient low-cost, available route for this aim.[4] Nano-sized magnetic nanoparticles and their hybrids or composites with clay materials have received increasing attentions as adsorbents for removal of organic pollutants from water sources due to high surface area and large adsorption capacity.[5] Organoclay is a membrane of clay materials with silica sheets constructing from two basic tetrahedral and octahedral units, which have been modified by organic groups. They are cheap, readily available materials, which can be used to adsorb contaminants from environment. Their structure has a negative charge, which can easily attract and hold cationic pollutants and eliminate them from aqueous solutions.[6, 7]

In order to improve and reinforce the physical and chemical properties of clay materials, nano-sized inorganic particles can be introduced to the body of clays.[8, 9] Among various fillers, magnetic nanomaterials have attracted a lot of attention due to special properties.[10, 11] Magnetic nanoparticles dispersed in clay matrix, in addition to expand the adsorption capacity *via* electrostatic interactions lead to the simplicity of their recovery from workplaces. In fact, magnetic adsorbents can be employed to remove the pollutants in water and after operation can be absolutely separated from environment by their magnetic properties. On the other side, the tendency of magnetic nanoparticles to the agglomeration leads to increase their particle size and decrease their activities as adsorbent or catalyst.[12] As a new feasibility, the encapsulation of magnetic metal oxides inside clay body can prevent the agglomeration and therefore, produce a new class of nanocomposites with a small particle size and high surface area. Amongst magnetic materials, spinel ferrites, MFe_2O_4, especially $ZnFe_2O_4$ are technologically introduced as an important class of nanomaterials due to their magnetic,[13] catalytic,[14] photocatalytic, [15] optical and electrical properties.[16-18] Hence, there is a great potential for

their application in the synthesis of magnetic nanohybrid and nanocomposite adsorbents for dealing with the environmental problems.[19] On the other hand, the discovery of new, low cost and innovative procedures to prepare the single phased magnetic nanomaterials according to the required demands is of great importance to devise technologies for the mass production. The most of the described synthesis methods in literature for the pure phase preparation of zinc ferrites require to a high temperature of calcination, severe experimental conditions, complex equipments and demand several steps, special chemicals.[20-22] Among reported methods such as co-precipitation,[23] hydrothermal/solvothermal,[24, 25] mechanochemical,[26, 27] sol-gel[28], thermal decomposition,[29] *etc.,* combustion technique assisted by microwave energy has attracted a lot of attention due to its simplicity, cost effective, quick and short time reaction. Despite the conventional combustion (that its heat is generated from an external heating source *e.g.,* a hot filament), in the microwave assisted process heating energy is internally resulted from the reactants-microwave interaction. In this process, throughout work-piece is exposed by the microwave energy, opened the combustion reaction and prepared product.[30-34] However this technique is simple and quick, the sintering or calcination post reaction and also, the supply of the enough energy for this operation is appeared to be an important subject. Therefore, it is necessary to modify the employed technique to tackle the problems for the synthesis of a pure phase of magnetic $ZnFe_2O_4$. Since a single-phased magnetic structure having the fascinating performance can be a good candidate for embedding in the matrix of composites and applying in water purification, we designed and performed a new method for the synthesis of zinc ferrite nanomaterial in this work. As an innovative idea, we designed one step reaction of solid state combustion assisted by microwave heating energy *via* constructing the reaction set-up encircled by a jacket of microwave absorber layer in walls and one preventer fiberglass layer in floor. This strategy can convert the absorbed microwaves to heat and create calcinating conditions without using any

external heat source. It means that the use of microwave absorber material, CuO, leads to center microwave heating energy and engineers the best conditions for the rapid preparation of pure phased zinc ferrite in nanoscale. As a noted, the use of a microwave absorbing layer in microwave assisted techniques to supply the sufficient heating energy to form a pure phase of product by one step reaction has not been yet reported. On the other hand, because such technique is operated in solid state without any organic solvents, it can be introduced as an environmentally friendly method.

Many different approaches have been reported to fabricate metal oxide/clay nanocomposites such as co-precipitation, molecular self-assembly, sol gel processing, *etc*.[35-37]A few works have been reported for this aim using ultrasound assisted procedure, while it is an effective, rapid and facile procedure to prepare uniform structures in the range of materials technology.[11] This technique is a reliable and simple route, which easily provides a uniformity and reactivity by the atomic level mixing within the reaction system. In addition, ultrasound waves produce the effective droplets and the adequate mechanical force leading to the better dispersion of species in aqueous solution and the better exfoliation of organoclay layers for the encapsulation of magnetic nanoparticles. This technique not only is a simple and rapid method for the formation of zinc ferrite/organoclay nanocomposite but also open a new pathway for the synthesis of the various nanocomposites.

As objectives of this research, we synthesized a pure phase of zinc ferrite nanoparticles with an acceptable surface area by a simple and available technique without any additional treatment. Then, we successfully prepared $ZnFe_2O_4$/clay nanocomposite through dispersing magnetic nanoparticles in commercial exfoliated organoclay by a facile ultrasound assisted impregnation and promoted their adsorption behavior for water treatment. Malachite Green (MG) and Brilliant Green (BG) were selected as a model of dye pollutants for adsorption study at room temperature and natural pH.

2. Experimental

2.1 Materials

Iron (III) nitrate nonahydrate ($Fe(NO_3)_3.9H_2O$, 99%), zinc nitrate hexahydrate ($Zn(NO_3)_2.6H_2O$, 99%), urea (CH_4N_2O, 99%), glycine (Gly, NH_2CH_2COOH, 99%) and ammonium nitrate ($(NH_4)(NO_3)$, 99%) were purchased from Merck Co. and used without further purification. Commercial-grade organoclay with the purity of 95% was purchased from Sahand Petroplastic International Co. (Iran). Brilliant green ($C_{27}H_{33}N_2.HO_4S$) and Malachite green ($C_{23}H_{25}ClN_2$) dyes were purchased from commercial sources as model dyes. Distilled water was used to prepare all solutions.

2.2 Synthesis of $ZnFe_2O_4$ nanoparticles

Fe $(NO_3)_3.9H_2O$ and Zn $(NO_3)_2.6H_2O$ with the molar ratio of 2:1 were mixed to each other in the presence of Gly or urea and ammonium nitrate as fuel and driving agents with different molar ratio to obtain the optimal conditions. The mixture was transferred into the designed reaction set-up and put into a domestic microwave oven with regulated power from 300 to 900 W (33%, 66% and 100% of power and 2450 MHz) for tunable time of 5-20 min. After the treatments, the voluminous sponge-like products were collected, washed with distilled water and ethanol several times to remove the residual initial materials, centrifuged, dried at 80 °C overnight and then, analyzed. The effect of fuel change and also, the effect of variation of power and time on the formation of product were also discussed in detail. The structural and morphological studies were carried out using FT-IR, XRD, SEM, EDX, VSM and BET analyses.

2.3 Reaction set-up

In order to produce the clacination conditions in microwave oven without any external thermal source, we designed and manufactured a reaction set-up with the ability of absorbing and transforming the microwaves to high temperature heat energy. Fig. 1 illustrates a scheme of this

reaction set-up. It has made up from an alumina crucible with a jacket of CuO layer in around to absorb microwave energy and produce calcination heat. A thick fiberglass layer was embedded in floor of container in outside to prevent the heat transfer to the bottom and probable damages to the glass plate of oven.

2.4. Synthesis of $ZnFe_2O_4$/organoclay nanohybrid

The as-prepared magnetic zinc ferrite nanoparticles (180 mg) were dispersed and entrapped into organoclay suspension in water (20 mg, 50 mL) by ultrasound waves with power of 200 W for 2 h. Then, the sediment was collected, washed with deionized water several times and dried at 80 °C for 16 h. Finally, the brown colored powder was obtained and studied the structure and characteristics of this product.

2.5 Characterization techniques

Fourier transform infrared (FT-IR) spectra were recorded on a Shimadzu-8400S spectrometer in the range of 400–4000 cm^{-1} using KBr pellets. The X-ray diffraction (XRD) patterns were recorded by a STOE powder diffraction system using Cu Kα radiation (wavelength, λ = 1.54060 Å). Scanning electron microscopy (SEM) images were taken on a Hitachi S4160 FESEM with gold coating and energy-dispersive X-ray spectroscopy analysis (EDX) on a VEGA\\ TESCAN S360 with gold coating. A double-beam UV spectrophotometer (Shimadzu UV-1700) was used for determination of dyes concentrations in the supernatant solutions before and after adsorption. The magnetic property was recorded using a vibrating sample magnetometer (VSM, MDK6) which has been made by the efforts of the Magnetis Daghigh Kavir Company in Iran. The surface area of the final product was obtained by using Brunauer-Emmett-Teller (BET) technique with Micromeritics (Gemini) in the range of relative pressures from 0.0 to 1.0. Before

employing, the sample was degassed at 473 K for 2 h. Microwave radiation was supplied using a domestic microwave oven with a controllable power and time (LG model, 2450 GHz).

2.5 Adsorption Process

To study the adsorption behavior of the prepared samples, Malachite Green (MG) and Brilliant Green (BG)) were selected as a model of dye pollutants (the molecular structure in Scheme S1 of supplementary data). The adsorption experiments were performed *via* treating 50 mL of MG and BG dyes solutions with the initial concentration of 20 to 200 mg L^{-1} with introducing 0.02 g of zinc ferrite nanoparticles and zinc ferrite/organoclay nanohybrid as adsorbent at room temperature and neutral pH for 4 h in dark.

The residual concentrations of dyes were measured using UV–Vis spectrophotometer at appropriate wavelengths corresponding to the maximum absorptions of BG (624 nm) and MG (617 nm).

3. Results and Discussion

3.1. The structural description of the prepared products

Fig. 2a indicates the recorded FT-IR spectrum from the resulting zinc ferrite nanoparticles after reaction using Gly/ammonium nitrate method in the power of 900 W for 20 min. The peaks at 417 and 550 cm^{-1} are attributed to the vibration frequencies of Zn^{2+}– O and Fe^{3+}– O bands, respectively.[15] Due to the suitable calcination conditions supplied by reaction set-up having a microwave absorbing jacket of CuO material, all of organic sections were easily removed and only metal-oxygen bands remained. It was observed that without application of this absorber jacket at the same conditions, the peaks at 831, 1381 and 1634 cm^{-1} are appeared (Fig. 2b). They are clearly related to vibration frequencies of the organic functional groups existent in product, which are corresponding with C-O bending and stretching vibrations, C=O stretching vibration

frequency overlapped with O-H bending of H_2O molecules, respectively. Meanwhile, the observed broad band at the range of 3150-3400 cm^{-1} can be assigned to the stretching vibration frequencies of ammonium and hydroxyl groups of precursor.[38] However fuel and nitrate groups in combustion process can produce a high temperature of reaction and oxidation, it is inadequate to synthesize a pure phased zinc ferrite at short time. While, the use of copper oxide layer as a microwave absorber material produces the more qualified conditions for the formation of single phased sample.

The similar X-ray diffraction patterns were obtained for the resulting products in both of the designed urea/nitrate (Fig. 3a) and Gly/nitrate (Fig. 3b) models. XRD patterns confirmed the formation of single spinel phase of $ZnFe_2O_4$ with a lattice parameter a= 8.446 Å. The all diffraction peaks at 2θ values of 18.17º, 29.89º, 35.21º, 36.83º, 42.78º, 46.84º, 53.07º, 56.57º, 62.11º, 70.44º, 73.45º and 74.44º are in a close agreement with the crystalline planes of 111, 220, 311, 222, 400, 331, 422, 511, 440, 620, 533 and 622 from the cubic system of zinc ferrite (JCPDS- 01-079-1150). No other peaks related to the impurities were detected.

Fig. 4 indicates the SEM images and histogram graphs of the prepared magnetic samples by utilizing glycine/ammonium nitrate (a-b) and urea/ammonium nitrate (c-d) as fuel/driving agent in the mentioned optimal conditions. These images revealed a nano-sized particulate morphology of both products with the uniformity in distribution and the average particle size of 32 and 41 nm in Gly/ nitrate and urea/ nitrate routes, respectively. Although an agglomeration of nanoparticles is observed in SEM images, which is due to magnetic property of the synthesized zinc ferrite particles and being tiny size of them, the uniform spherical morphology of product is clear. The histograms (Figs 4e and f) of the particles size distribution for the resulting products were determined by microstructure measurement program and Minitab statistical software. It was

observed that Gly burns the better than urea during combustion reaction due to the flash point of 176 °C and therefore, it can be a more appropriate fuel for preparing zinc ferrite nanoparticles. Scheme 1 shows a graphical illustration of production process of the magnetic nanoparticles and escape of gases molecules, which can create pores between particles.

Elemental analysis by EDX shown in Fig. 5 and ICP data demonstrated the presence of Zn, Fe elements. These data indicate the exact concentration of iron and zinc elements in the resulting product so that the calculated ratio of iron to zinc is in a close accordance with the stoichiometrical ratio of 2 that expected.

The nitrogen adsorption-desorption experiments were carried out to determine the surface area of the prepared magnetic product under optimal conditions. The recorded adsorption and desorption isotherm curves (Fig. 6) with a distinct hysteresis loop similar to the category of type IV represented the meso-porous nature of the resulting product with the Langmuir surface area of 82.13 m^2g^{-1}. This value is considerable for magnetic metal oxides synthesized by solid state reaction and indicates the presence of the high contact sites on the surface of specimen. The pore size distribution of the resulting nanoparticles was evaluated by Barrett–Joyner–Halenda (BJH) model using desorption branch of the nitrogen isotherm (in the inset of Fig. 6). This plot illustrated that the pore size distribution for this product is centered at 4.8 nm.

To study the influence of reaction time and power of irradiation on the resulting nanopartciles, we performed a series of experiments using urea/nitrate and also Gly/nitrate models at the different times and powers. The portions of solid solutions were taken away from the reaction set-up at the intervals of 5, 10 and 15 min under identical conditions and analyzed. In addition, the effect of power parameter on the structure and morphology of product was investigated by declining the irradiation power to 600 and 300 W. The observation of some peaks of the organic

sections in recorded FT-IR spectra (Supporting Information Figs. S1a and b, respectively) clearly indicated that the combustion reaction has not completely developed and the pure phased structure for final magnetic product is failure to appear. The XRD patterns also demonstrated the aforementioned FT-IR data (Supporting Information of Fig. S2). An overview of these data indicates the incomplete growth of the crystalline system and particulate morphology, the decrease in crystallinity and so the formation of deficient products. It seems that the decline of reaction time or power results the unqualified and inadequate energy and so reaction conditions for preparing single phased zinc ferrite. Although, the XRD patterns for the Gly/nitrate model (Figs. S3 of supplementary data) indicated a small change by the time and power variation, the SEM images introduced the operation time of 20 min with the power of 900 W as an optimal reaction to synthesize magnetic zinc ferrite nanoparticles (Fig. 7).

Therefore, the microwave power of 900 W and operation time of 20 min into a reaction set-up encircled by a layer of microwave absorbing materials can be introduced as the optimal experimental conditions to produce pure single phased zinc ferrite.

In order to evaluate reproducibility and repeatability of the designed model for the synthesis of pure phased zinc ferrite nanoparticles, we performed the aforementioned technique three times and analyzed the resulting products by XRD and FT-IR techniques (Fig. 8). The results revealed a pure phase of ferrite material without any impurity for each three runs, which confirmed the suitability of this procedure to synthesize magnetic ferrite nanomaterials.

Another objective of this work is the synthesis of novel zinc ferrite/organoclay nanocomposite by introducing of zinc ferrite nanoparticles onto organoclay sheets by ultrasound assisted procedure. The capture of magnetic nanoparticles using clay layers can be a facile route to prevent the accumulation of magnetic nanoparticles and produce the novel nanocomposites with

the high efficient properties. We encapsulated the as-prepared magnetic zinc ferrite nanoparticles by organoclay layers *via* ultrasound assisted impregnation during 2 h and then, characterized.

The XRD patterns of the commercial organoclay and processed nanocomposite were shown in Fig. 9a. The reflection peaks of zinc ferrite nanoparticles are obviously observed in XRD pattern of the resulting sample confirming the successful incorporation of zinc ferrite nanoparticles with the clay sheets. In addition, the reflection peaks of the expanded low angle degree of XRD (LXRD) patterns for unprocessed organoclay (Fig. 9b-i) and as prepared composite (Fig. 9b-ii) were compared in detail. An obvious shift is observed at 2θ value of 6.9° and 3.3° in raw organoclay pattern to 2θ value of 4° and 1.4° in processed product pattern, respectively, which can be originated from entrapping some zinc ferrite nanoparticles within clay sheets. The interlayer spacing of ca. 12.6 and 22.7 Å were obtained for the employed organoclay and prepared zinc ferrite/organoclay nanohybrid, respectively. This noticeable expansion can be an evidence of successful encapsulation of zinc ferrite nanoparticles within organocaly sheets. Scheme 2 indicates a conceptual representation of the intercalation of zinc ferrite nanoparticles into the interlayer of organoclay.

The magnetic property of such prepared products was determined by vibrating sample magnetometer (VSM) with the highest applied field of 10 kOe at room temperature (Figs. 10). In general, normal spinel zinc ferrite with the general formula of AB_2O_4 is an antiferromagnetic material in nature and can show a paramagnetic behavior in nano-scale at room temperature. However its normal spinel structure consists of the tetrahedral A (Zn^{2+}) sites and octahedral B (Fe^{3+}) sites, it can be partially inverted. Thus, a fraction of Fe^{3+} out of preferred octahedral sites are tetrahedrally coordinated by the oxygen atoms, which can lead to increase the magnetic features of zinc ferrite.[39-41] The magnetization (M) versus the applied magnetic field (H) for

resulting nanoparticles at room temperature lightly indicated an S-like shape of magnetic characteristic with the magnetization of 2.6 emu/g and no saturation with the available maximum field (Fig. 10a). It can be resulted from the irregular structure of surface-spin in the prepared nanoparticles. Meanwhile, the magnetic features can change with the decrease of particle size to nano-scale, which is influenced by synthesis techniques. Therefore, an appeared little paramagnetic behavior for the prepared product is describable due to these arguments. It was found that the encapsulation of these magnetic nanoparticles by the organoclay sheets leads to increase the paramagnetic properties of product due to the separation of particles and distribute on the clay sheets, uniformly (Fig. 10b). Due to the observed coercivity (Hc) of the close to zero, the prepared products are soft-magnetic materials.

The SEM images shown in Figs. 11a-b revealed the layered morphology of the produced nanocomposite. Meanwhile, EDX analysis from raw clay and produced sample (Fig. 11c) confirmed the presence of Zn and Fe elements of zinc ferrite in the prepared composite and revealed the encapsulation of 82% of magnetic zinc ferrite nanoparticles with the nanoclay particles in the resulting sample. The morphology of the prepared nanohybrid at 82 wt% of zinc ferrite particles in the composite was studied by TEM technique (Fig. 12). The blurry image observed in images probably is due to the possible interference of the electron beam caused by the magnetism of ferrite particles. The presence of spherical magnetic nanoparticles embedded in the layered structure of clay body is clearly observed in TEM images. Based on these results, it can be proposed that zinc ferrite particles have been distributed into clusters and located outsides the clay interlayer galleries, which lead to create a meso-porous architecture by stacking of clay layers. The adsorption and desorption isotherm curves for the commercial organoclay (Fig.S4 of supplementary data) and the prepared nanocomposite (Fig. 13) revealed a hysteresis loop in the

range of 0<P/P0<1, which is in a close accordance with the category of type IV, which represents the meso-porous nature for the final product. BET analysis by using nitrogen adsorption-desorption experiments indicated the surface area of 65.2 m^2/g for the resultant nanocomposite. The Barrett–Joyner–Halenda (BJH) model using desorption branch of the nitrogen isotherm was employed to determine the pore size distribution of this product. BJH plot (in the inset of Fig. 13) revealed a uniform pore size distribution centered at 6.7 nm. These data illustrated a decrease of pore size diameter of raw organoclay from 15 nm to 6.7 nm for the prepared nanohybrid. It probably is due to the encapsulation of zinc ferrite nanoparticle into the silicate layers of organoclay body. These experimental findings present that the synthesized magnetic nanocomposite can be nominated as an efficient adsorbent for the adsorption of organic colored contaminants in water. Since the adsorption process by magnetic nanomaterials is a simple method to remove the colored contaminants from aqueous solutions, this part has been devoted to this matter. In order to investigate this feature, we selected toxic MG and BG dyes as a model of colored pollutants and carried out adsorption experiments by introducing the prepared magnetic zinc ferrite nanoparticles and zinc ferrite/organoclay compound to dye solutions, separately in dark.

3.2. Adsorption behavior of the resulting products

The decolorizing percentage of the selected pollutants in water by adsorption mechanism is calculated by the following equation:

$$\%\ \text{Removal efficiency} = \frac{C_0 - C_t}{C_0} \times 100 \qquad \text{(Eq. 1)}$$

The contact time for the adsorption of dye molecules was studied *via* performing a series of adsorption experiments for the prepared nanocomposite at the range time of 1-5 h. As a result, the suitable time to remove the selected contaminants at neutral pH was obtained, which revealed

the maximum removal efficiency after 4 h. After this time, the adsorption percentage is constant, *i.e.,* the surface of adsorbents saturates by the adsorption of dye molecules and this leads to decrease the adsorbing percentage. (Fig. S5 of supplementary data). Therefore, agitation time of 4h was selected for further studies.

The adsorption isotherms of Langmuir (Eq. (2)) and Freundlich (Eq. (3)) are commonly used to evaluate the adsorption process:

$$\frac{C_e}{q_e} = C_e\left(\frac{a_L}{K_L}\right) + \left(\frac{1}{K_L}\right) \qquad \text{(Eq. 2)}$$

$$\text{Log } q_e = \text{Log } K_F + \frac{1}{n} \text{ Log } C_e \qquad \text{(Eq. 3)}$$

where, a_L (Lmg^{-1}) and K_L (Lg^{-1}) are the Langmuir constants. These constants are calculated from the slope and intercept of the plot between C_e/q_e and C_e. Meanwhile, K_F ($mg^{1-1/n}\ L^{1/n}\ g^{-1}$) and n are the Freundlich adsorption isotherm constants, which are obtained from the slope and intercept of linear plot of Log q_e *vs.* Log C_e. These adsorption isotherms are employed to elucidate the interactions between dye molecules and adsorbent. In these equations, C_e is the equilibrium concentration of pollutant in solution (mg L^{-1}), q_e is the amount of dye molecules adsorbed (mg g^{-1}) per unit of adsorbent at equilibrium (mg g^{-1}), which is calculated by the equation (4):[34]

$$q_e = \frac{V(Ci - Cf)}{m} \qquad \text{(Eq. 4)}$$

Where, C_i and C_f are the initial and final concentrations of contaminant in mg L^{-1}, respectively. V is the volume of experimental solution in L, and m is the weight of adsorbent in g.

Fig. 14 shows the plots of Langmuir (Fig. 14a) and Freundlich (Fig. 14b) adsorption isotherms for the obtained nanocomposite. The Langmuir and Freundlich adsorption isotherms plots of the magnetic zinc ferrite nanoparticles have been given in Fig. S6 of supporting information. The

parameters of the Langmuir and Freundlich adsorption isotherms were calculated and given in Table 1. The calculated correlation coefficients (R^2) indicated that Langmuir model is in a better agreement than the Freundlich model for the adsorption process by the synthesized nanocomposite. The results of zinc ferrite indicated that these species also follows the Langmuir model.

In fact, the Langmuir equation as an adsorption isotherm model can describe the relationship between the amount of adsorbed dye molecules on magnetic adsorbents and its equilibrium concentration in solution. Although, this model does not consider the variation in adsorption energy, it obviously describes the adsorption method. It is based on the physical theory that the maximum adsorption capacity (q_{max}) includes a monolayer adsorption.[42]The maximum adsorption capacity (mg g^{-1}) is obtained by [$q_{max} = K_L/a_L$]. The calculated values of q_{max} have been given in Table 1. The results revealed that the maximum values of adsorption capacity (q_{max}) belong to the adsorption of MG and BG pollutants by composite sample. In fact, this compound represented the remarkable adsorption efficiencies for selected dye pollutants. This ability can be originated from the increase of contact sites between adsorbent and adsorbed molecules on the surface of nanocomposite by inserting zinc ferrite nanoparticles to the clay architecture. Clay materials indicate a strong attraction for adsorption of both cationic and anionic dyes and a good capability to uptake dyes in water. Fig. 15 suggests a schematic adsorption mechanism of dye pollutants onto the prepared nanocomposite. The intercalation of zinc ferrite nanoparticles within organoclay galleries and formation of magnetic nanohybdrid probably lead to create a large number of charge groups on the clay surface which invigorates the electrostatic attraction between the positively charged dyes and negatively charged surface of composite. Therefore, dye molecules can easily enter into the clay matrix and interact with

composite surface, results into the formation of ionic complex and increases the dye removal from aqueous solution.

In fact, the electrostatic and hydrogen bonds interactions act as the driving forces of adsorption process. One such operation is governed by the large number of contact sites on the nanohybrid surface so that the as-prepared $ZnFe_2O_4$/organoclay nanocomposite exhibits higher adsorption capacity than the prepared zinc ferrite and unprocessed clay. As shown in Fig. 16, the FT-IR spectra of the nanocomposite before (Fig. 16a) and after adsorption of BG (Fig. 16b) and MG (Fig. 16c) dye pollutants indicated the bands of Zn^{2+}–O and Fe^{3+}–O at 460 and 520 cm^{-1}, respectively that reveal the zinc ferrite existence in composite matrix. The presence of strong vibration bands at the range of 900-1100 cm^{-1} in all FT-IR spectra before and after adsorption are related to the Si-O stretching bands of clay material in composite body. The appeared peaks at 1350-1575 cm^{-1} after adsorption of dye molecules can be ascribed to the aromatic groups of dye skeleton adsorbed on the composite surface. In addition, the absorption bands at the range of 3400-3600 and 1640 cm^{-1} are corresponding to –OH stretching and bending vibrations of adsorbed H_2O molecules on the composite surface, respectively. In addition, the peaks of –CH symmetrical and asymmetrical stretching vibration at 2850 and 2920 cm^{-1} are strengthened after adsorption of dye species. These FT-IR data were also obtained for adsorption of BG and MG dye pollutants by zinc ferrite nanoparticles (shown in Fig. S7 of supplementary data, BG and MG FT-IR spectra have been shown in the inset of this Fig.).The results clearly suggest the formation ionic complex of dye/nanohybrid during adsorption process which increases the dye removal.

As shown in Fig. 17 the reusability of this nanocomposite for the adsorption of selected dye pollutants was studied by designing a series of experiments and zinc ferrite/organoclay particles

were reused three times under similar conditions. Before each experiment, the adsorbent was collected, centrifuged, washed with ethanol and deionized water several times to remove the adsorbed species, dried, and performed again. The results presented not much more decrease in the decolourizing efficiency, which demonstrates the stable behavior of this product for further adsorption cycles for the water treatment.

4. Conclusions

In a brief, we successfully prepared magnetic $ZnFe_2O_4$ nanoparticles and $ZnFe_2O_4$/organoclay nanocomposite with the considerable surface areas by a new and facile technique. We presented an innovative strategy to synthesize the magnetic zinc ferrite nanoparticles by modifying the combustion assisted procedure. This technique can open a new window to synthesize the pure phase of various nano-sized ferrites with a great potential in industrial applications. In addition, magnetic nanocomposite was easily obtained *via* encapsulating the resulting nanoparticles by organoclay sheets using ultrasound assisted method. The study of adsorption performance of the resulting products revealed a superior capability of nanocomposite compared with the zinc ferrite nanoparticles for water treatment by adsorption mechanism. The magnetic properties for recovery operation and proper surface area can nominate the prepared nanocomposite as an excellent adsorbent for water purification.

Acknowledgements

The financial support from Iran University of Science and Technology (IUST) and Iranian Nanotechnology Initiative is gratefully acknowledged.

References

1 L. Han, X. Zhou, L. Wan, Y. Deng and S. Zhan, *J. Environ. Chem. Eng.*, 2014, **2**, 123.

2 D. Lu, Y. Zhang, S. Lin, L. Wang and C. Wang, *J. Alloys Compd.*, 2013, **579**, 336.

3 E. Dvininov, E. Popovici, R. Pode, L. Cocheci, P. Barvinschi and V. Nica, *J. Hazard. Mater.*, 2009, **167**, 1050.

4 N. V. Kaneva and C. D. Dushkin, *Colloids Surf., A*, 2011, **382**, 211.

5 B. S. Kadu and R. C. Chikate, *Chem. Eng. J.*, 2013, **228**, 308.

6 L. G. Yan, X. Q. Shan, B. Wen and S. Zhang, *J. Colloid Interface Sci.*, 2007, **308**, 11.

7 L. Ai, Y. Zhou and J. Jiang, *Desalination*, 2011, **266**, 72.

8 I. Fatimah, *J. Adv. Res.*, 2014, **5**, 663.

9 A. Dhakshinamoorthy, P. Visuvamithiran, V. Tharmaraj and K. Pitchumani, *Catal. Commun.*, 2011, **16**, 15.

10 X. Ma, F. Xu, L. Chen, Z. Zhang, Y. Du and Y. Xie, *J. Cryst. Growth*, 2005, **280**, 118.

11 S. R. Shirsath, A. P. Hage, M. Zhou, S. H. Sonawane and M. Ashokkumar, *Desalination*, 2011, **281**, 429.

12 T. Szabó, A. Bakandritsos, V. Tzitzios, S. Papp, L. Korösi, G. Galbács, K. Musabekov, D. Bolatova, D. Petridis and I. Dékány, *Nanotechnology*, 2007, **18**, 285602.

13 C. Yao, Q. Zeng, G. F. Goya, T. Torres, J. Liu, H. Wu, M. Ge, Y. Zeng, Y. Wang and J. Z. Jiang, *J. Phys. Chem. C*, 2007, **111**, 12274.

14 S. W. Cao, Y. J. Zhu, G. F. Cheng and Y. H. Huang, *J. Hazard. Mater.*, 2009, **171**, 431.

15 Y. Fu, X. Wang, *Ind. Eng. Chem. Res*., 2011, **50**, 7210.

16 R. Dom, R. Subasri, K. Radha and P. H. Borse, *Solid State Commun.*, 2011, **151**, 470.

17 M. Sultan and R. Singh, *J. Appl. Phys.*, 2009, **105**, 07A512.

18 H. Xu, X. Chen, L. Chen, L. Li, L. Xu, J. Yang and Y. Qian, *Int. J. Electrochem. Sci.*, 2012, **7**, 7976.

19 C.-H. Chen, Y.-H. Liang and W.-D. Zhang, *J. Alloys Compd.*, 2010, **501**, 168.

20 J. P. Singh, G. Dixit, R. C. Srivastava, H. M. Agrawal, V. R. Reddy and A. Gupta, *J. Magn. Magn. Mater.*, 2012, **324**, 2553.

21 S. D. Jadhav, P. P. Hankare, R. P. Patil and R. Sasikala, *Mater. Lett.*, 2011, **65**, 371.

22 X. Bo, G. Li, X. Qiu, Y. Xue and L. Li, *J. Solid State Chem.*, 2007, **180**, 1038.

23 Y. Zhang, Q. Shi, J. Schliesser, B. F. Woodfield, Z. Nan, *Inorg. Chem.,* 2014, **53**, 10463.

24 F. Liu, X. Chu, Y. Dong, W. Zhang, W. Sun and L. Shen, *Sens. Actuators, B*, 2013, **188**, 469.

25 R. Shao, L. Sun, L. Tang and Z. Chen, *Chem. Eng. J.*, 2013, **217**, 185.

26 V. Nachbaur, G. Tauvel, T. Verdier, M. Jean, J. Juraszek and D. Houvet, *J. Alloys Compd.*, 2009, **473**, 303.

27 H. Yang, X. Zhang, C. Huang, W. Yang and G. Qiu, *J. Phys. Chem. Solids*, 2004, **65**, 1329.

28 M. Mumtaz, S. Naeem, K. Nadeem, F. Naeem, A. Jabbar, Y. R. Zheng, N. A. Khan and M. Imran, *Solid State Sci.*, 2013, **22**, 21.

29 C. Yao, Q. Zeng, G. F. Goya, T. Torres, J. Liu, H. Wu, M. Ge, Y. Zeng, Y. Wang, J. Z. Jiang, *J. Phys. Chem. C,* 2007, **111**, 12274.

30 S. Gedevanishvili, D. Agrawal and R. Roy, *J. Mater. Sci. Lett.*, 1999, **18**, 665.

31 H. Parmar, R. V. Upadhyay, S. Rayaprol and V. Siruguri, *Indian J. Phys.*, 2014, **88**, 1257.

32 B. Reeja-Jayan, K. L. Harrison, K. Yang, C.L. Wang, A. E. Yilmaz, A. Manthiram, *Sci. Report*, 2012, **2**, 1.

33 R. Rosa, C. Ponzoni, C. Leonelli, *Inorganics,* 2014, **2**, 191.

34 Y. V. Bykov, K. I. Rybakov, V. E. Semenov, *J. Phys. D: Appl. Phys*., 2001, **34**, 55.

35 R.S. Hsu, W.H. Chang, J.J. Lin, *Appl. Mater. Interface.,* 2010, **2**, 1349.

36 H.Mao, X. Liu, J. Yang, B. Li, Q. Chen, J. Zhong, *Microporous Mesoporous Mater.,* 2014, **184**,169.

37 H. Mao, X. Liu, J. Yang, B. Li,C.Yao,Y. Kong, *Mater. Sci. Eng. C*, 2014, **40**,102.

38 K. Nakamoto, Infrared Raman Spectra of Inorganic and Coordination Compounds, 6th ed., John Wiley & Sons, Inc., Hoboken, New Jersey, 2009.

39 T. Xie, L. Xu, C. Liu, Y. Wang, *Appl. Surf. Sci.,* 2013, **273,** 684.

40 T. Sato, K. Haneda, M. Seki, T. Iijima, *Appl. Phys. A,* 1990, **50**, 13.

41 F. Grasset, N. Labhsetwar, D. Li, D. C. Park, N. Saito, H. Haneda, O. Cador, T. Roisnel, S. Mornet, E. Duguet, J. Portier, J. Etourneau, *Langmuir,* 2002, **18**, 8209.

42 A. Afkhami, R. Moosavi, *J. Hazard. Mater.,* 2010, **174**, 398.

Figure captions

Fig.1. Schematic diagram of the reaction set-up.

Fig.2. FT-IR spectra of the resulting products by the designed technique using microwave absorber jacket (CuO) **(a**) and without CuO (**b**).

Fig.3. XRD patterns of the prepared $ZnFe_2O_4$ by urea/nitrate model (a) and Gly/nitrate model (b).

Fig.4. SEM images of the prepared $ZnFe_2O_4$ nanoparticles using Gly/NH_4NO_3 (**a-b**) and urea/ NH_4NO_3 (**c-d**), the statistical graph of particle size distribution of product prepared by Gly/NH_4NO_3 (**e**) and urea/ NH_4NO_3 (**f**).

Fig.5. EDX analysis of the resulting zinc ferrite nanoparticles.

Fig.6. Nitrogen adsorption (▲) and desorption (■) isotherm for resulting zinc ferrite nanoparticles. The inset shows BJH plot of this product.

Fig.7.SEM images of the prepared product using Gly/nitrate model in the reaction time and power of 5 min, 900 W (**a-b**), 10 min, 900 W(**c-d**), 15 min, 900 W (**e-f**), 20 min, 300 W (**g**) and 20 min, 600 W (**h**).

Fig. 8. XRD patterns for the resulting zinc ferrite nanoparticles after three times of reaction runs. The inset shows FT-IR spectra of these products.

Fig. 9. XRD patterns of the commerical organoclay (**a-i**) and zinc ferrite/clay nanocomposite (**a-ii**). The expanded low angle degree of XRD (LXRD) patterns of the raw clay (**b-i**) and prepared nanocomposite (**b-ii**).

Fig.10. The M–H hystersis loops for the prepared $ZnFe_2O_4$ nanoparticles (**a**) and $ZnFe_2O_4$/organoclay nanocomposite (**b**).

Fig. 11. SEM images of zinc ferrite/clay nanocomposite (**a-b**) and EDX nanlysis (**c**) of this product.

Fig. 12. TEM images of the prepared zinc ferrite/organoclay nanocomposite.

Fig. 13. Nitrogen adsorption (▲) and desorption (●) isotherm for the prepared nanocomposite. The inset shows BJH plot of this product.

Fig. 14. The plots of Langmuir (Figs. 13a-i and a-ii) and Freundlich (Figs. 13b-i and b-ii) of produced nanocomposite for the adsorption of BG and MG dye pollutants.

Fig. 15. A schematic proposed adsorption diagram of dye pollutants onto the prepared nanocomposite.

Fig. 16. FT-IR spectra of as prepared $ZnFe_2O_4$/organoclay nanocompiste before (a) and after adsorption of BG (b) and MG (c) dye pollutants.

Fig. 17. A diagram of reusability of the prepared zinc ferrite/organoclay nanocomposite for adsorption of the selected dye pollutants during three treatment times.

Table 1. Parameters of Langmuir and Freundlich isotherm equations, correlation coefficients (R^2) for adsorption of BG and MG dyes on the synthesized samples at 25 ˚C and neutral pH.

		Langmuir model				Freundlich model		
Dye		a_L (L mg^{-1})	K_L (L g^{-1})	q_{max} (mg g^{-1})	R^2	K_F ($mg^{1-1/n} L^{1/n} g^{-1}$)	n	R^2
The resulting nanocomposite	BG	0.11	45.24	384.61	0.98	60.78	1.97	0.95
	MG	0.19	46.94	238.09	0.99	78.68	3.74	0.85
The prepared Zinc ferrite	BG	0.30	23.80	76.92	0.98	0.63	0.43	0.91
	MG	0.32	21.05	64.10	0.98	7.68	2.40	0.94

Scheme

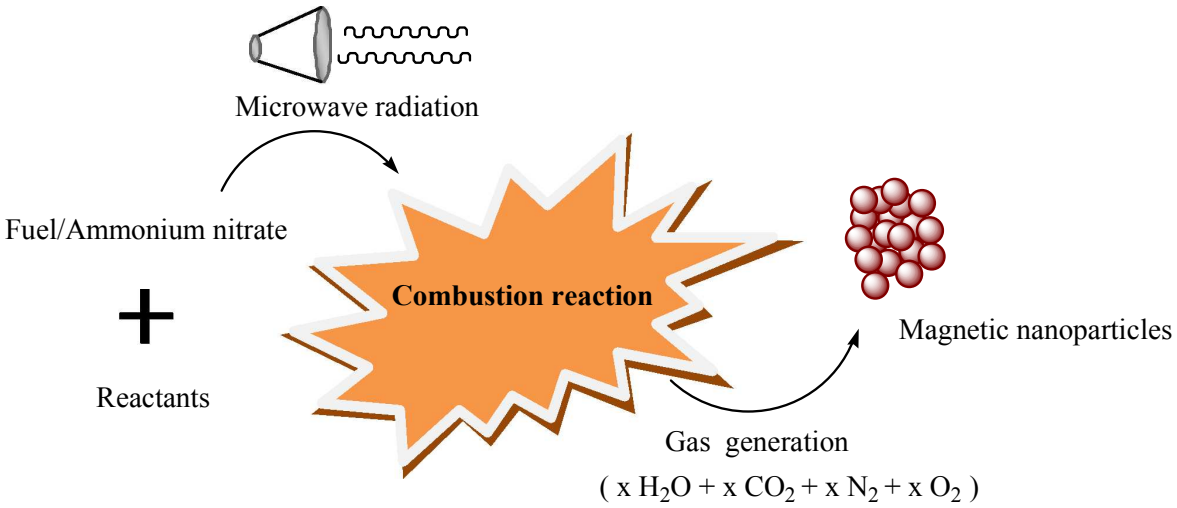

Scheme 1. The illustration of production process of magnetic zinc ferrite nanoparticles.

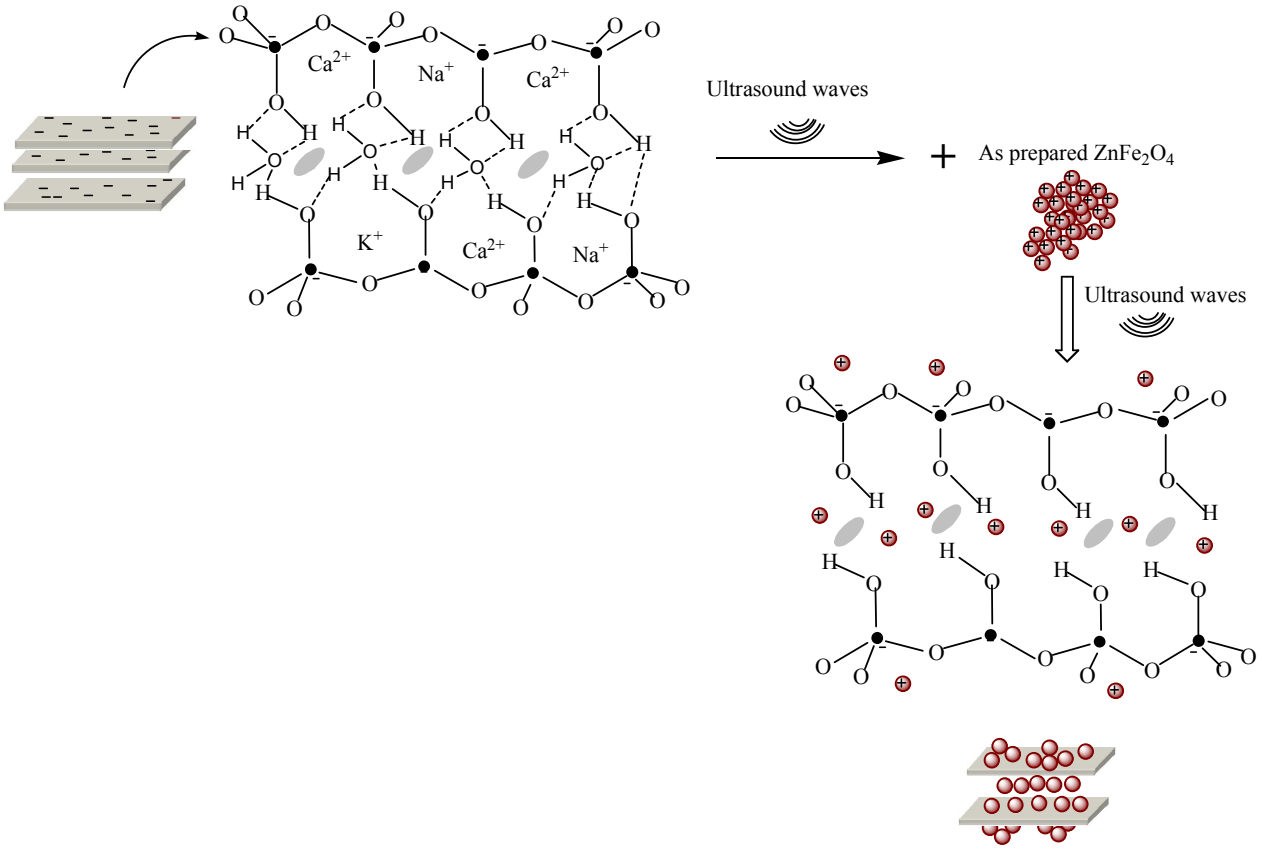

Scheme 2. A conceptual illustration of the intercalation of zinc ferrite nanoparticles into the interlayer of organoclay.

Figures

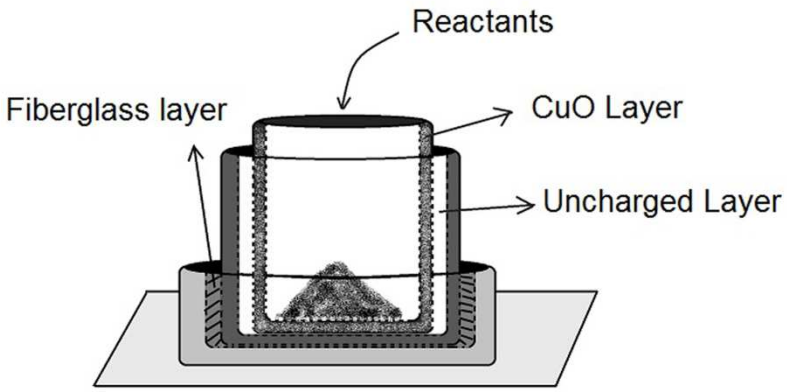

Fig. 1.

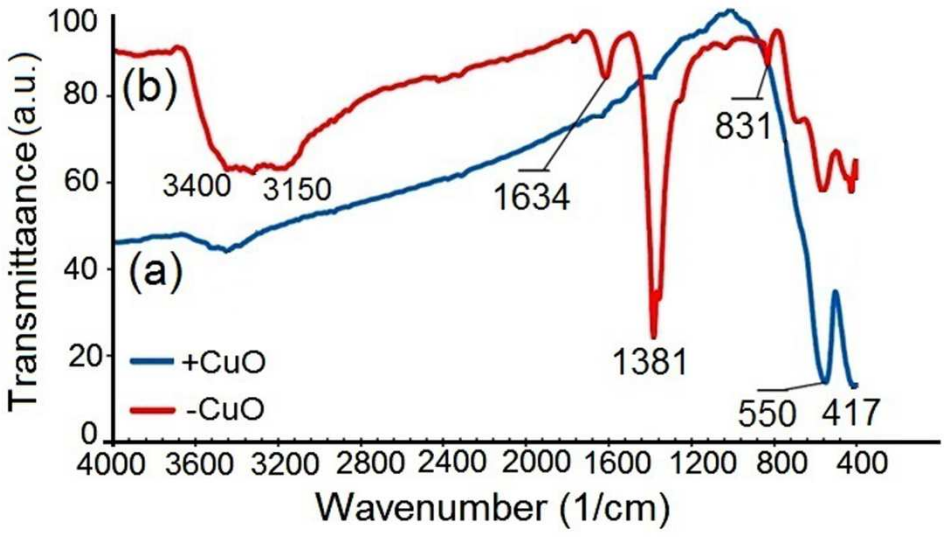

Fig. 2.

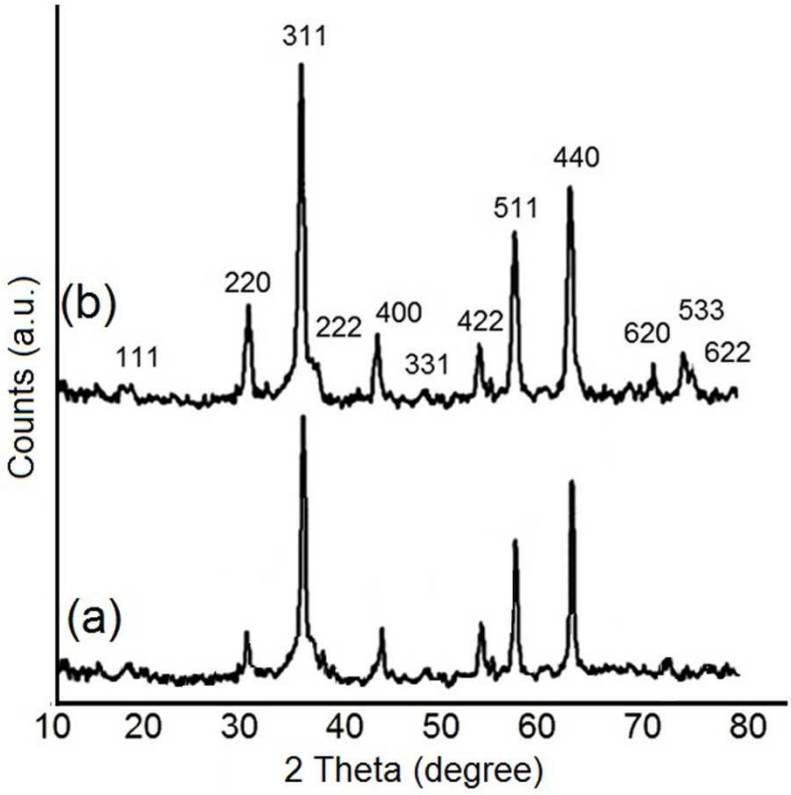

Fig. 3.

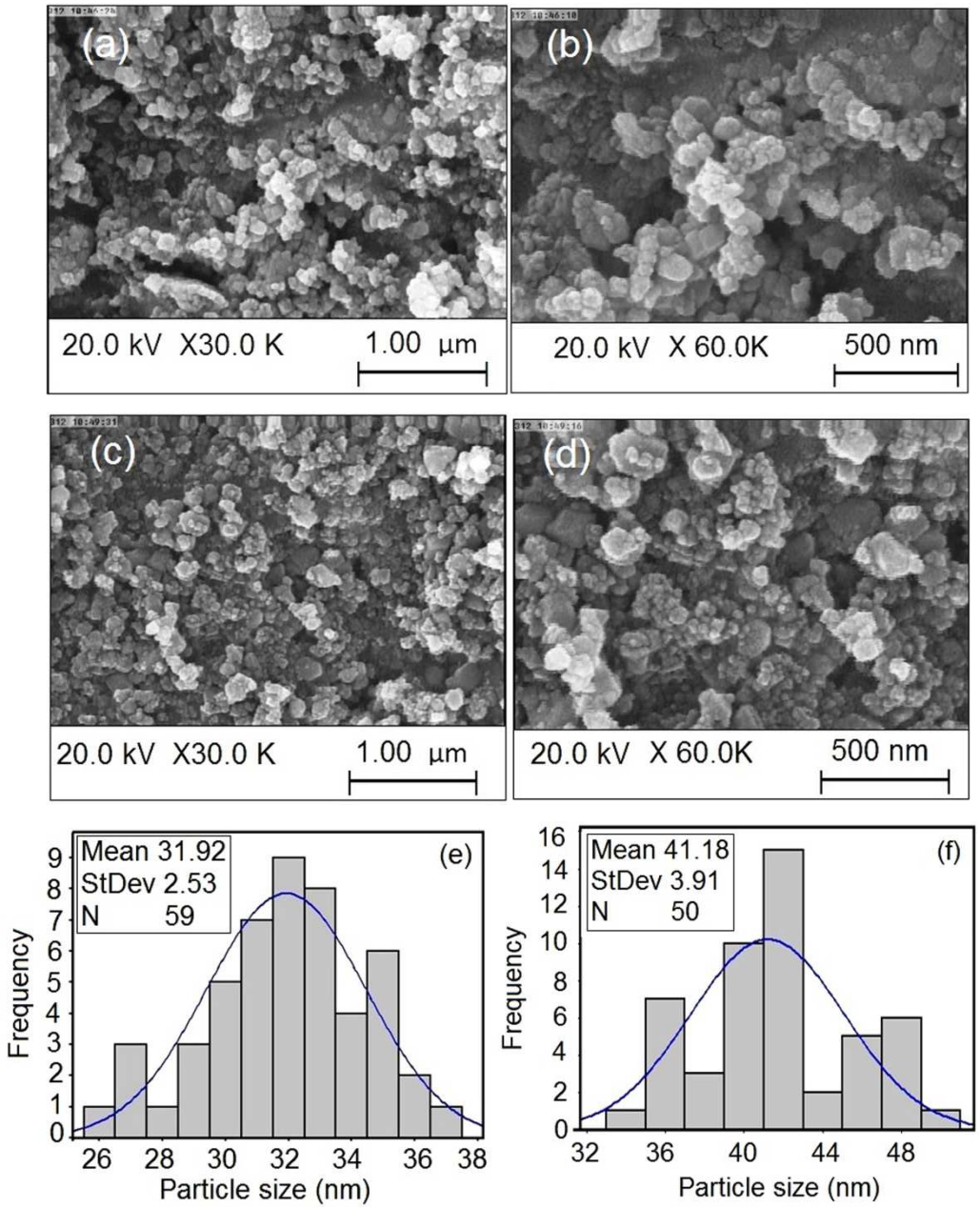

Fig. 4.

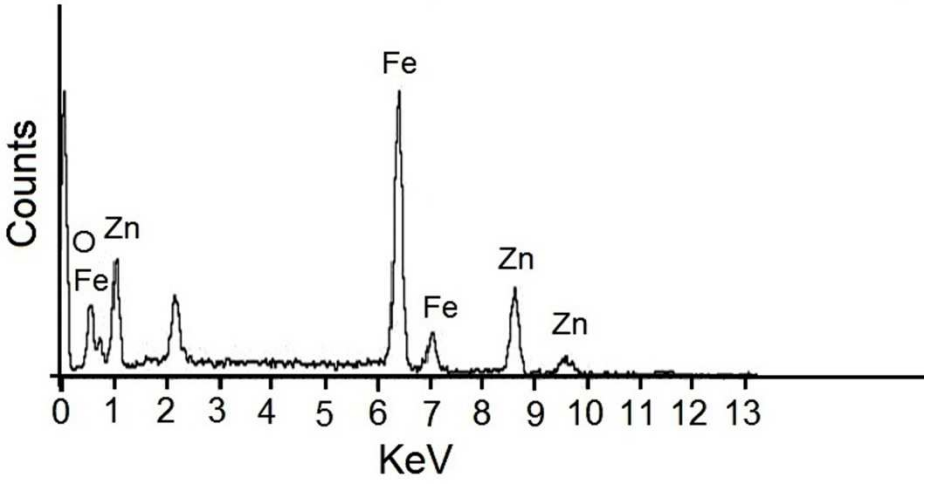

Fig. 5.

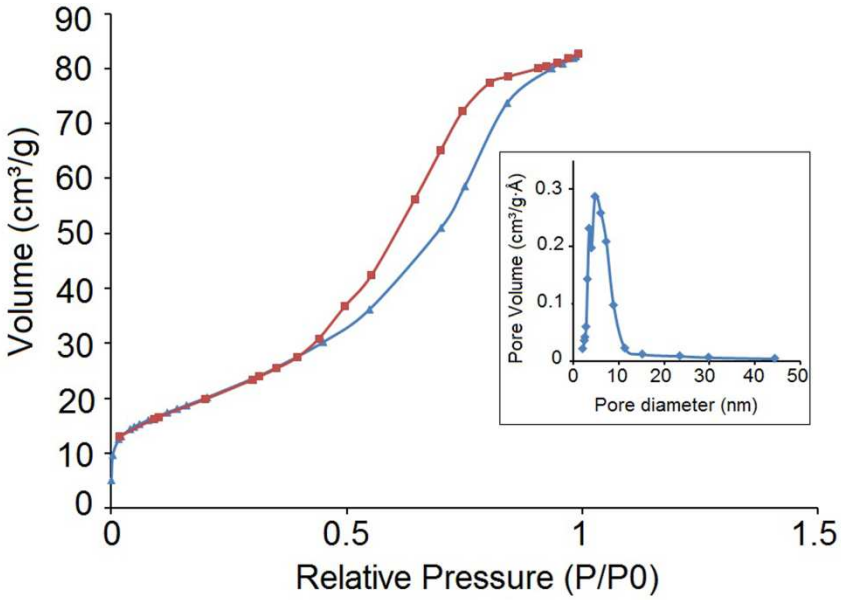

Fig. 6.

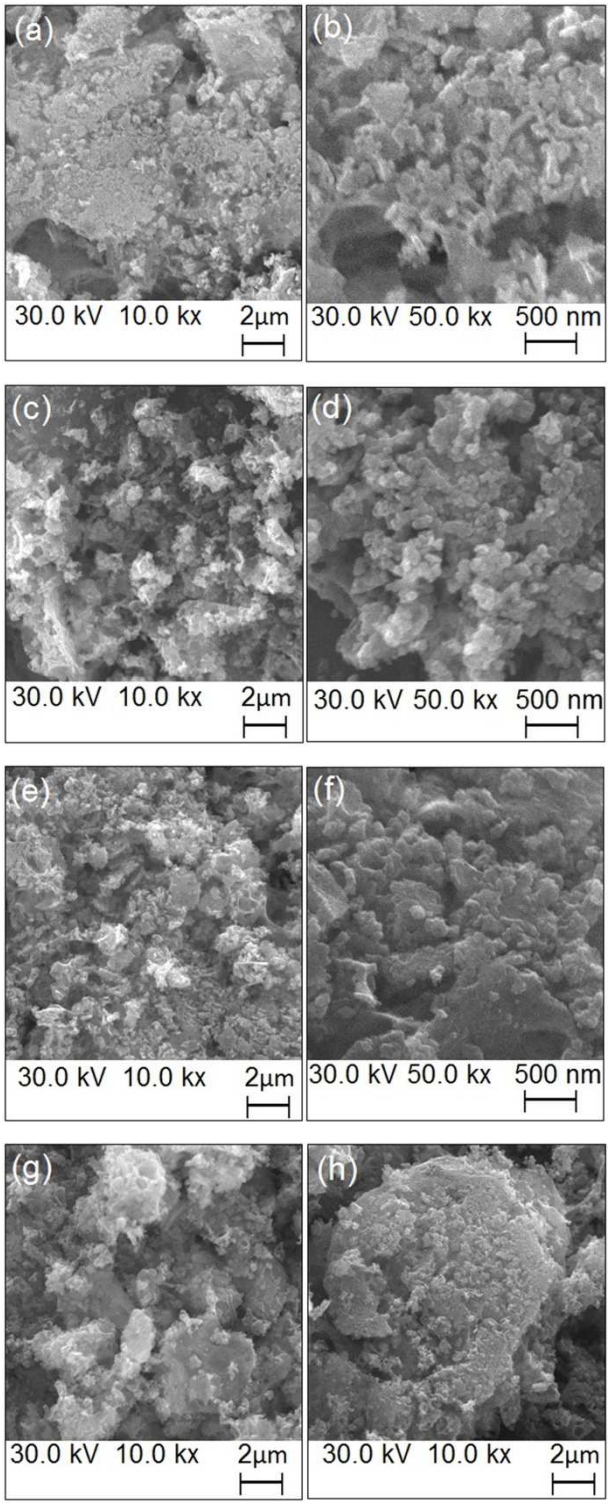

Fig. 7.

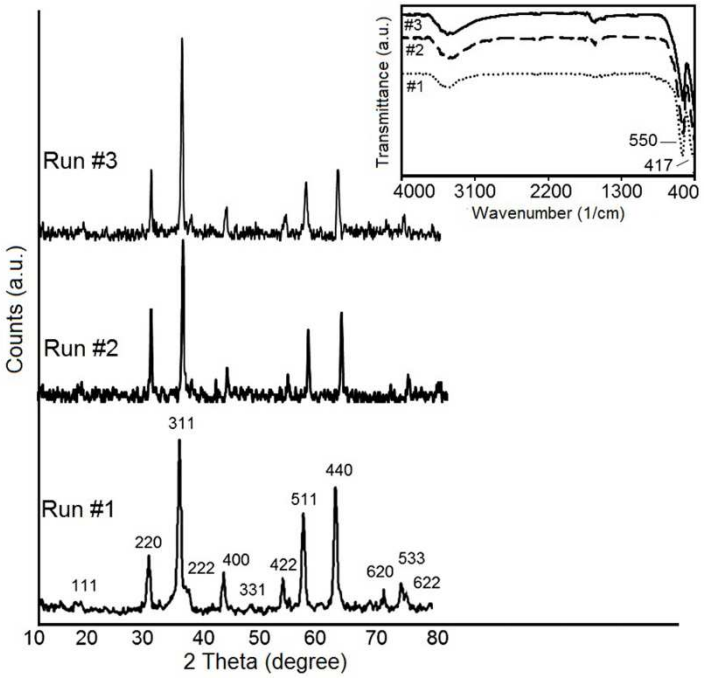

Fig. 8.

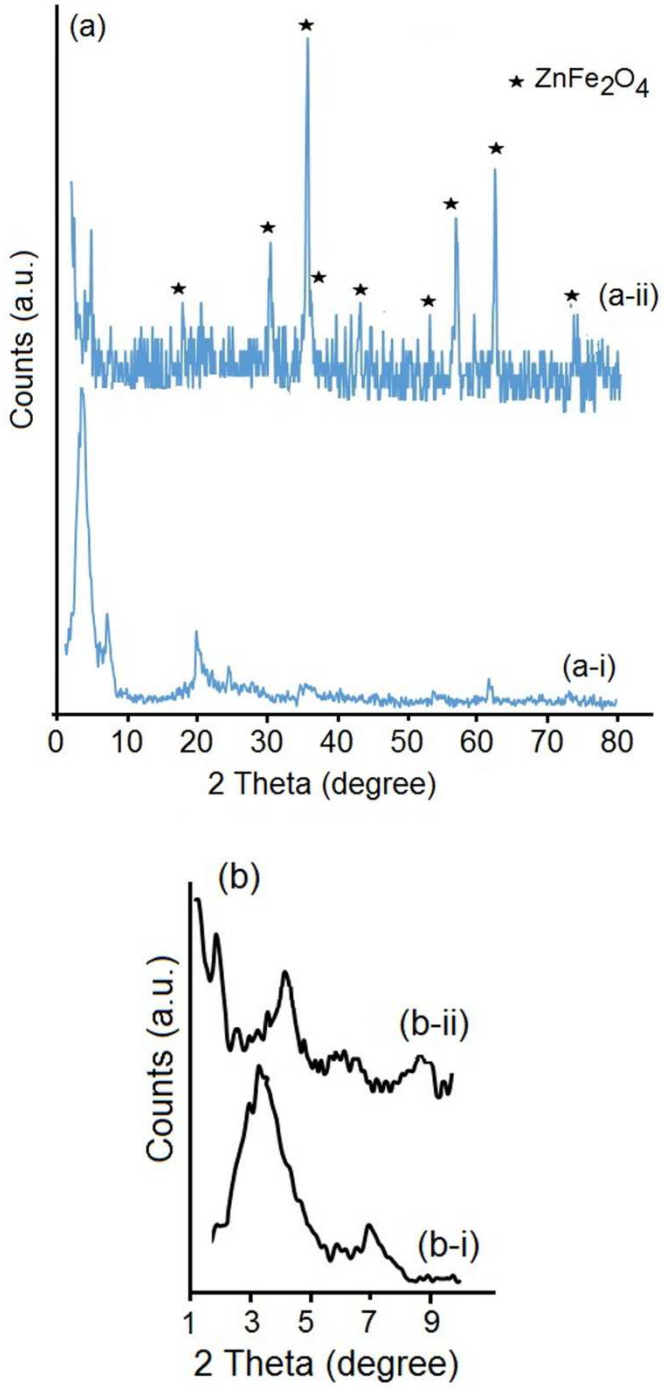

Fig. 9.

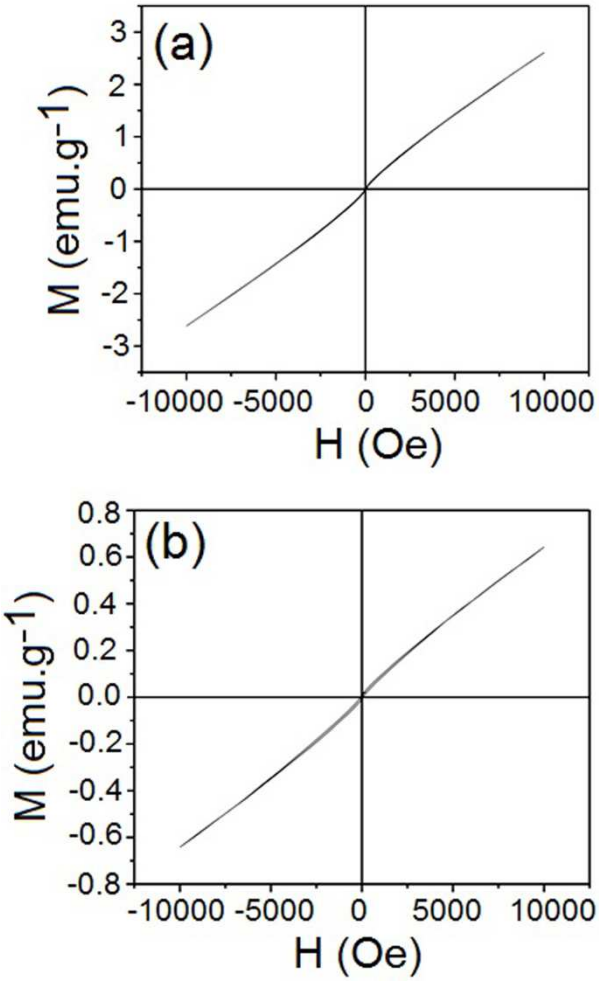

Fig, 10.

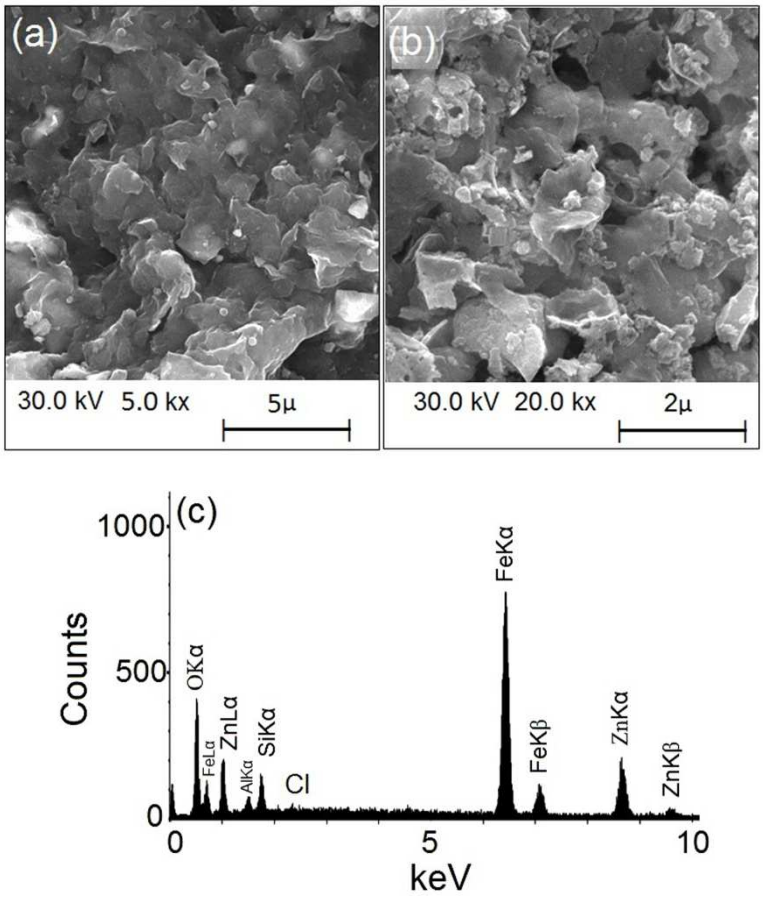

Fig.11.

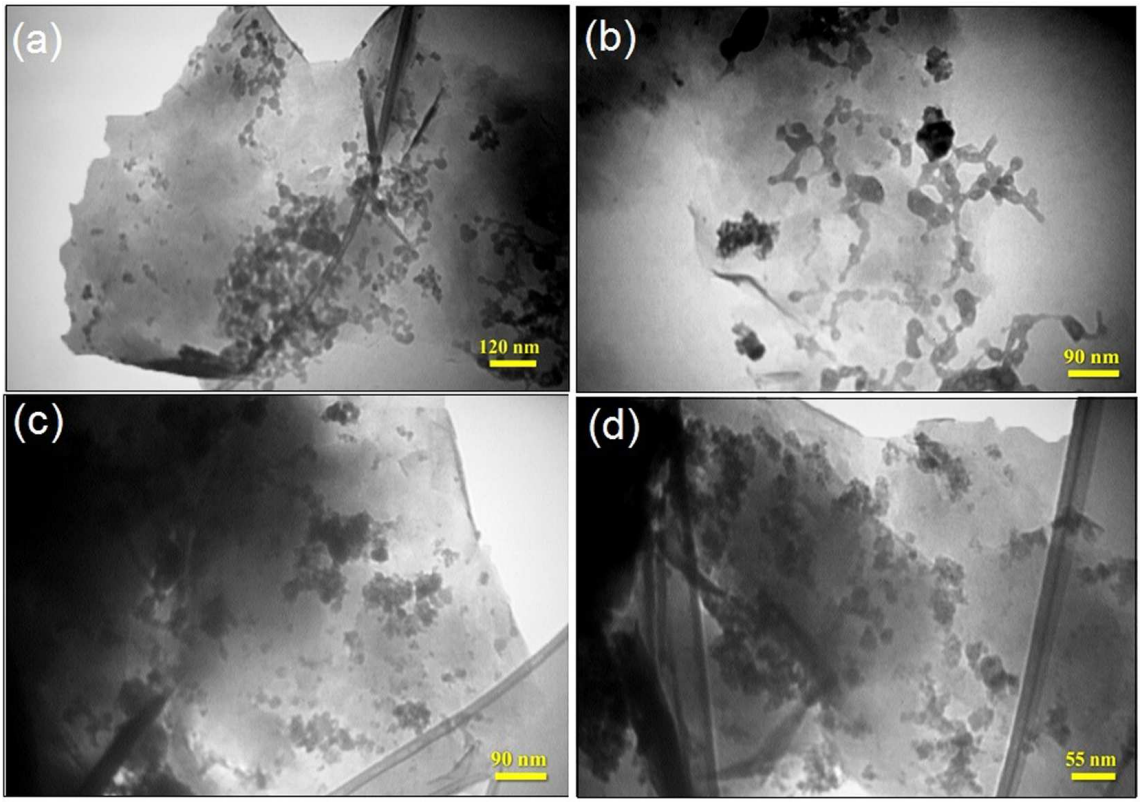

Fig. 12.

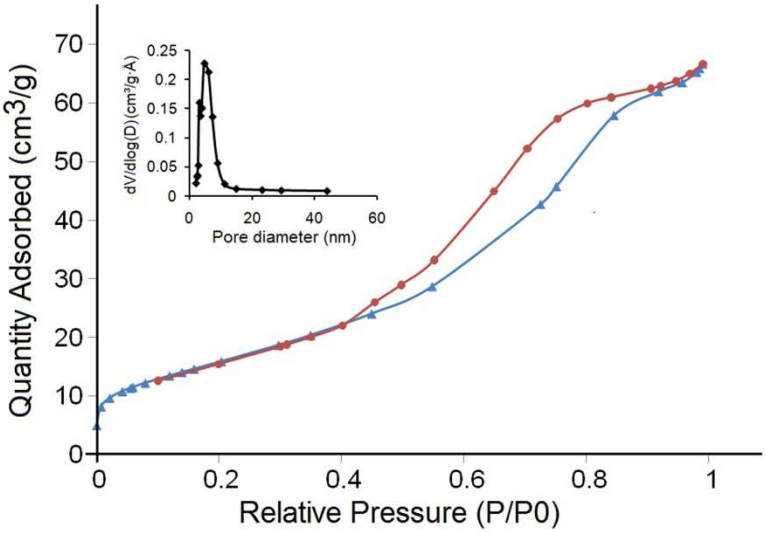

Fig. 13.

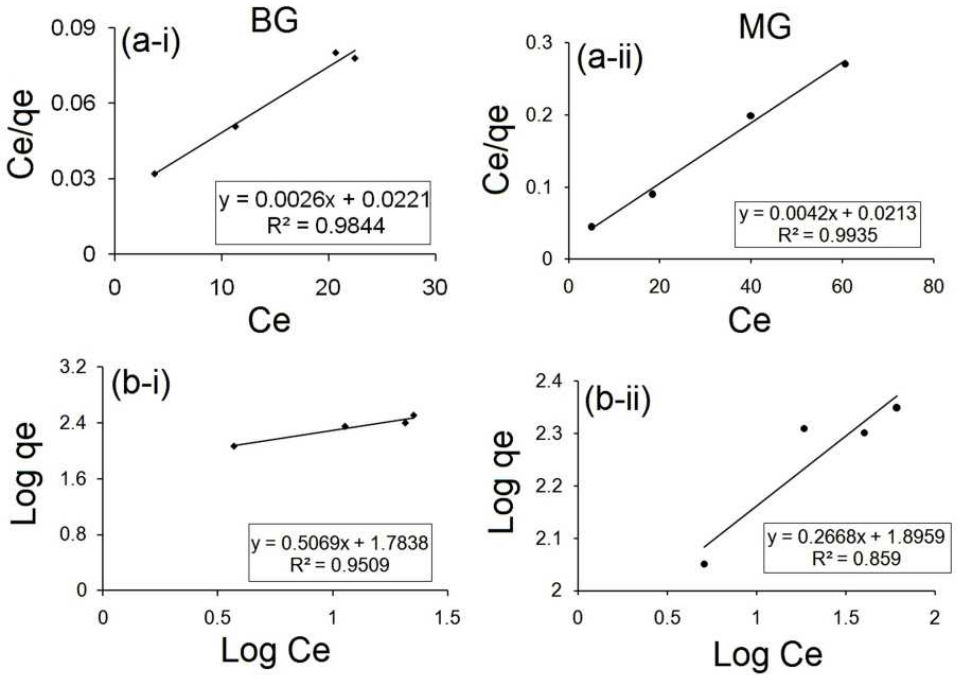

Fig.14.

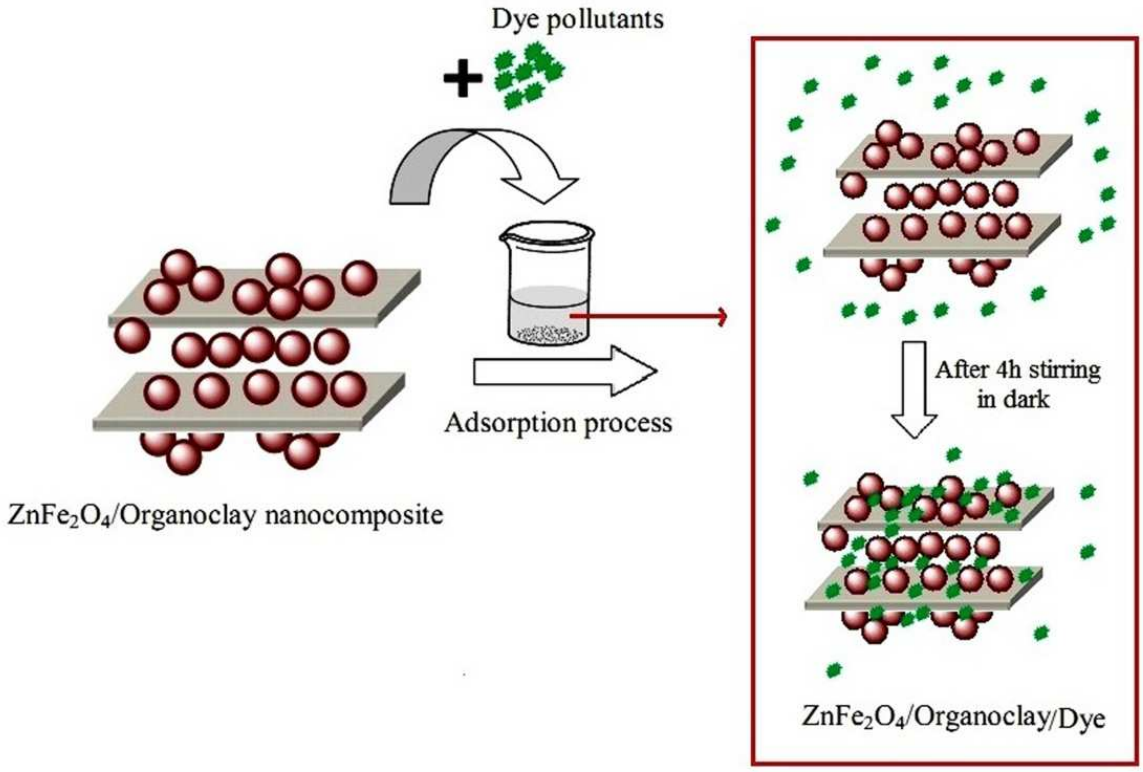

Fig. 15.

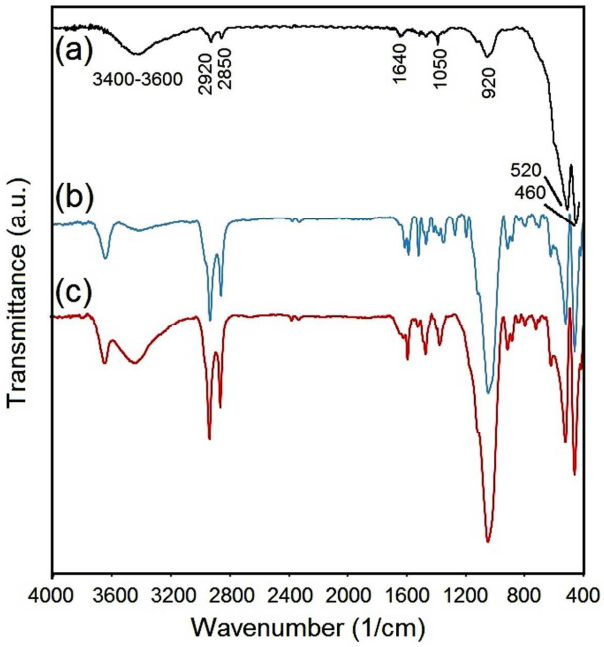

Fig. 16.

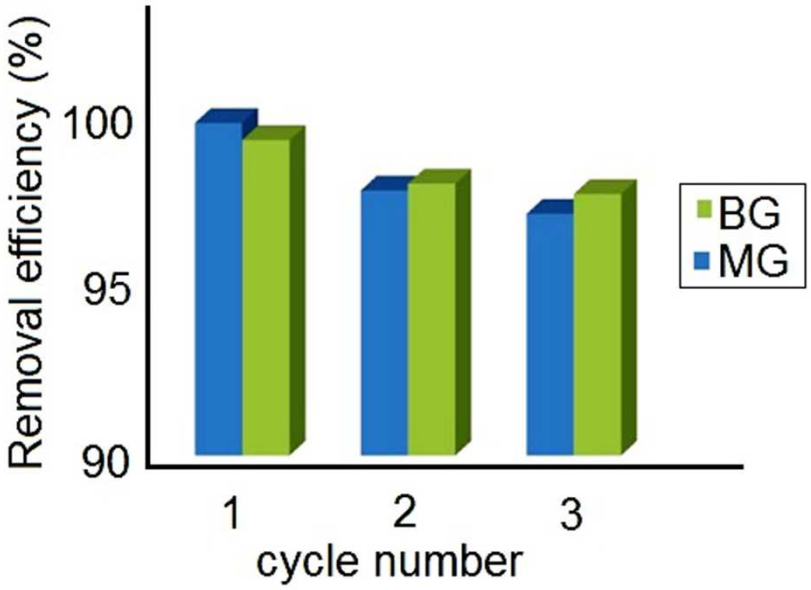

Fig. 17.